Effect of different types of wing-wing interactions in flapping MAVs

W.B. Tay[1]

[1]Temasek Laboratories, National University of Singapore, 5A Engineering Drive 1, 117411, Republic of Singapore

Abstract

Wing-wing interaction (WWI), such as the clap and fling motion (CFM), occurs when two wings are flapping in close proximity of one another. Due to the interactions between the wings and their vortices, improvement in the wing's performance can be obtained. We intend to design a hovering 4-wing flapping MAV (FMAV) which makes use of WWI to improve its lift performance at Re = 5,000 (based on chord length), through the use of numerical simulations. In this study, the objectives include 2 (TL_FMAV2) / 4-wing (TL_FMAV4) WWI comparison and the effect of different types of flexibility on lift and drag. Results show that TL_FMAV4 produces more than twice the amount of lift compared to TL_FMAV2, but at the expense of higher drag and power requirement. Investigations on wing flexibility found that having a rigid spanwise and flexible chordwise wing produces the highest lift, minimum drag and power requirement. These results will be beneficial in the understanding of the underlying aerodynamics of WWI.

Introduction

Wing-wing interaction (WWI) occurs when two wings are flapping in close proximity of one another. Due to the interactions between the wings and their vortices, improvement in the wing's performance can be obtained. One of the well-known wing-wing interaction is the clap and fling motion (CFM), which was first coined by Weis Forgh [1]. Another variation of the CFM is the clap-and-peel motion (CPM), where the "fling" is replaced by the "peel".

Our current interest lies in the design of a small FMAV best suited for hovering at Re ~ 5,000, with a maximum wingspan of 10cm, similar to the Delfly micro (the micro version of the Delfly [2]). It is called the "TL_FMAV4". The 10cm wingspan enables it to hover and maneuver in tight spaces. There is currently no FMAV which fits into this category. We intend to run simulations to characterize the effect of various parameters (such as kinematics, flexibility) on its performance. Most numerical simulations and experiments are mainly restricted to low or very low Re (8 – 1400). Hence, there is a need to investigate the flow field due to WWI at Re = 5,000. Due to the complexity involving simulations with membrane wings and FSI, as a preliminary step, we would like to investigate this unique 4-wing FMAV in a simplified form and from a more fundamental aspect. In this way, the effect of each parameter on the TL_FMAV4 can be clearly defined.

The default design configuration is based on the FW-MAV [3]. We would like to investigate the effect of WWI based on this configuration. There are two objectives we would like to achieve in this study. Firstly, is the 4-wing WWI compact configuration (TL_FMAV4) more advantageous compared to the 2-wing WWI (TL_FMAV2) configuration? Next, flexibility has been shown to reduce drag and increase lift [4]. However, the simulation was done in 2D and the current flapping configuration is very different

from the simulation. This prompt us to do a more definitive investigation in the area of flexibility. The simulations are performed in 3D, using the immersed boundary method (IBM) [5]. The reason for using IBM is because the wings come into close proximity of one another, a scenario whereby IBM is well suited for. The force, pressure and vorticity output from the results will be analyzed.

Numerical method

The WWI motion (WWIM) is simulated using the non-dimensional laminar Navier–Stokes equations using the fractional step method together with the IBM approach. The IBM approach is especially suited in this case because the wings are in close proximity of one another. The IBM solver has been validated against a 3D plunging wing experiment and successfully used to perform 3D simulations on the Delfly II model [6]. The reader may refer to the paper by Tay et al. [6] for part of the validation details, grid convergence study and application of the IBM solver. The current Re used in all the simulations is 5,000. The flow is laminar and hence no turbulence models has been added.

Simulation setup and grid convergence study

Figure 1 shows the 3D Cartesian grid with a pair of wings. A symmetry boundary condition is applied to the yz plane ($x = 0$) to mirror the other pair of wings to reduce the computational cost. The computational domain is 8×16×18 in the x, y and z-directions respectively. Grid convergence study, performed using the configuration WWIM1-px1_pz1[1], shows that a minimum grid length of $0.012c$ is sufficient. Refinement is used in the region near the wings and the resultant total number of cells for the domain is 248×494×364.
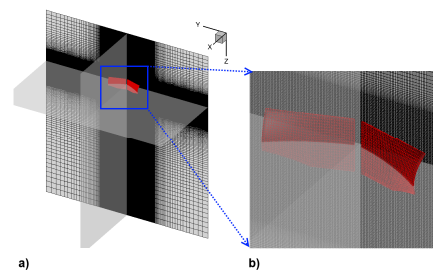

Figure 1. a) Normal and b) close-up isometric view of the Cartesian grid but the wings in red.

Research Methodology

The main objective is to gain a deeper understanding of WWI in the TL_FMAV4 from a fundamental aspect. We first discuss some restrictions and parameters which are fixed in order to adhere to

---

[1] The type of configurations will be explained in detail in the research methodology section.

the FMAV design. This is followed by the methodology to carry out the simulations to achieve the proposed objectives.

Wing, design parameters and restrictions

The wing shape in all simulations is the same as that of FW-MAV, as shown in Figure 2, with a maximum span and thickness of $1.5c$ and $0.03c$ respectively. The default horizontal and vertical distances (Δs) are fixed at $0.15c$, similar to that of Miller and Peskin [4].
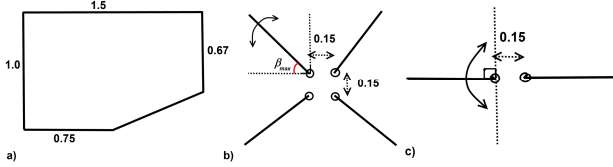

Figure 2. a) Planform of TL_FMAV4 wing, b) TL_FMAV4's top view and c) TL_FMAV2's top view. Lengths have been non-dimensionalized based in the root's chord length.

The root chord portion of the wing is fixed and hence during flapping, the prescribed rotation / deformation (α) of the wing tip causes the entire wing to twist and undergo spanwise and chordwise deformation, as shown in Figure 3. In the default 4-wing design, each wing flaps with an amplitude of $\beta_{max} = 45^o$. Referring to Figure 3, the default maximum chordwise deformation angle α_{max} is 44° (at wing tip).
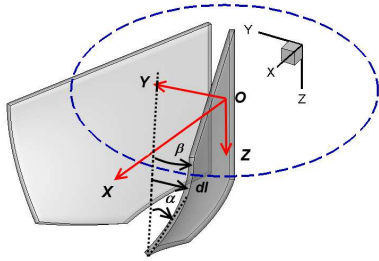

Figure 3. Isometric view of two of the four wings in the CFM. The other two wings not shown are located at the mirror image of the yz plane.

As mentioned earlier, the Re is 5,000. In the current hovering conditions, it is defined as:

$$\text{Re} = \frac{U_{ref}c}{\nu} \tag{1}$$

where U_{ref}, c and υ are the maximum tip velocity of the flapping wing, wing's chord length and kinematic viscosity respectively. The reduced frequency f_r is defined as:

$$f_r = \frac{fc}{U_{ref}} = 0.135 \tag{2}$$

where f is the actual flapping frequency. In hovering, f and U_{ref} are inter-related, with $\beta_{max} = 45^o$ to $f_r = 0.135$.

2-wing / 4-wing comparison study

The first objective is to compare the relative performance between the 2-wing and 4-wing FMAV design to determine if there is any real advantage in having a 4-wing FMAV (TL_FMAV4). The 2-wing FMAV (TL_FMAV2) is exactly the same as TL_FMAV4 except that it has two wings which flaps at twice the flapping angle of TL_FMAV4. The kinematics used in this comparison is the CFM because this motion has been used in many studies [7,8].

In the current 3D simulation, the translation and rotation become flapping (β) and deformation (α) respectively, as shown in Figure

3. Moreover, in this study, the starting time for both α and β is the same.

The parameters used for the 4-wing TL_FMAV4 has been discussed earlier. For the 2-wing FMAV (TL_FMAV2), the maximum flapping angle β_{max} now increases from 45° to 90°, as shown in Figure 2. Since the reduced frequency f_r depends on β_{max}, f_r now becomes 0.068. The two configurations will be compared side by side in terms of force output and power requirement.

Wing flexibility

In the introduction, it was mentioned that in CFM, adding flexibility to the wings (effectively becoming CPM) can reduce drag and improve lift [4]. The general conclusion is that under the right conditions, flexibility can be beneficial. However, each study platform is different and so the optimum conditions for each platform is different too. Hence, we would also like to assess the effect of flexibility on its performance under the current unique flapping configuration, Unlike other flexibility studies, the focus is not on the amount of flexibility, but on the difference between linear and quadratic deformation. To control the flexibility of the wings along the spanwise and chordwise directions, we vary the two constants px and pz. A value of 1 gives a linear variation along the span or chord, which is equivalent to a rigid deformation (fling), similar to the CFM. Hence, TL_FMAV4 is equivalent to the WWIM1-px1_pz1 configuration. On the other hand, a value of 2 gives a quadratic variation, equivalent to a flexible deformation (peel), as shown in Figure 4. The combinations of px and pz give four possible permutations, as given in Table 1.

Configuration type	px	pz	Simulation description
WWIM1-px1_pz1	1	1	WWIM1 with rigid spanwise, chordwise deformation
WWIM1-px1_pz2	1	2	Rigid spanwise, flexible chordwise deformation
WWIM1-px2_pz1	2	1	Flexible spanwise, rigid chordwise deformation
WWIM1-px2_pz2	2	2	Flexible spanwise and chordwise deformation

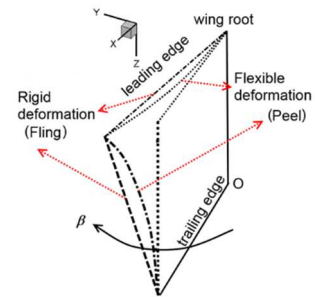Table 1. Configuration type with rigid or flexible span/chordwise deformation

Figure 4. Comparison between rigid and flexible deformation of the wing.

Results and discussions

TL_FMAV2/4 comparison

Figure 5 and Figure 6 show the c_l, c_{dx}, c_{dy} and P_{in} of one wing of TL_FMAV2 and TL_FMAV4 over one period. In comparison, the trend of the force and power requirement variation are very similar for both but the peak values of TL_FMAV2's force and power are much lower, due to its lower frequency. For ease of visualization and analysis, cylindrical sections of the 3D pressure field at radius $R = 1.25c$ is created and then projected on a plane. We focus our

attention on the pressure contours at four time instants $(a – d)$ in Figure 7. In the beginning, from (a) to (b), there is a large increase in lift for both TL_FMAV2 and TL_FMAV4. As shown in Figure 7a to b, this is due to the large pressure difference between the upper and lower surface of the wing as a result of the sudden fling motion. The peak lift for the latter is much higher since the pressure magnitude difference is larger. However, this also creates high drag and power requirement in TL_FMAV4, as shown in Figure 5 and Figure 6. At time = 0.08T (b), the lift is decreasing due to the formation of the TEV for both cases. At time = 0.12T (c), the lift of TL_FMAV2 is larger than that of TL_FMAV4, as the former's TEV has shed. This vortical asymmetry maintains the lift and prevents it from decreasing sharply, unlike in TL_FMAV4 case. The clap motion happens at time = 0.40T (d), when the lift increases again sharply for both cases. Similarly, the large pressure difference between the upper and lower surface of the wing of TL_FMAV4 produces a much higher lift peak, compared to that of TL_FMAV2. Since both TL_FMAV2 and TL_FMAV4 undergo symmetrical motion when flapping inwards and outwards, the lift variation repeats itself after every half cycle.

Comparing the overall performance of the TL_FAV2 and TL_FMAV4, the four wings of TL_FMAV4 produces $\bar{c_l} = 4\times0.15 = 0.60$, while the two wings of TL_FMAV2 produces only $\bar{c_l} = 2\times0.13 = 0.26$, less than half that of TL_FMAV4. However, the $\bar{P_{in}}$ of TL_FMAV4 is also more than double that of TL_FMAV2 (0.96 against 0.32). Similarly, the maximum drag force of TL_FMAV4 is also higher (3.46 against 1.38). Based on the above results, it now comes to the question whether if it is worthwhile designing a 4-wing FMAV. This should depend mainly on the mission objective. If the payload requirement of the FMAV is low while its endurance requirement is high, then TL_FMAV2 may be more suitable, since its power requirement is lower than that of TL_FMAV4. However, in most surveillance or search-and-rescue missions, there are payloads, such as sensors and camera. Assuming that the weight increase in moving from TL_FMAV2 to TL_FMAV4 is comparatively small (10 – 20%), the 2× more lift production can offset the weight increase and higher payload. If required, a larger battery can be used to improve its endurance as well. In addition, TL_FMAV4 is just as compact in size as TL_FMAV2.
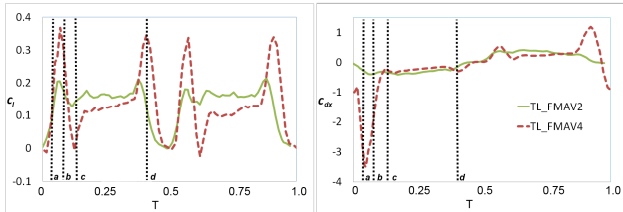

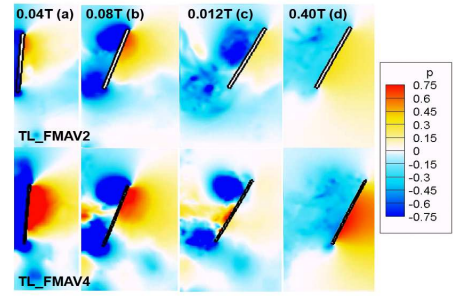Figure 7. Projected pressure contours of TL_FMAV2 / 4 at radius = 1.25c at four time instants. (a) to (d) correspond to the time instants of the vertical dotted lines in Figure 5 and Figure 6.

Effect of wing flexibility

In this section, the effect of wing flexibility is investigated by varying the deformation along the span and chord of the wings. Despite the subtle difference (linear or quadratic) in the deformation, results between them can be very different. Comparison of the Q criterion iso-surface of the wings with different flexibility at two time instants is shown in Figure 8. At time = 0.12T, LEVs of wings with spanwise quadratic flexibility $(px = 2)$ have detached while LEVs of those with spanwise rigid flexibility $(px = 1)$ are still attached at their roots. At time = 0.32T, LEVs of wings with $px = 2$ have re-attached. On the other hand, the root LEV of the wing with $px = 1$ has spiralled out into a long and thin vortex. This shows that even subtle flexibility can have a large influence on the evolution of the LEV.
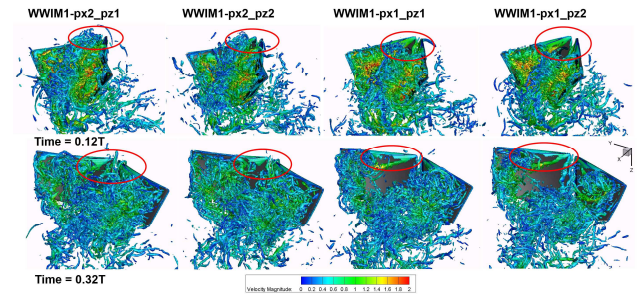

Figure 8. Vortex structures, color-coded with velocity magnitude, of WWIM1-px2_pz1, px2_pz2, px1_pz1 and px1_pz2 at Q criterion (Q) = 50 at two time instants.
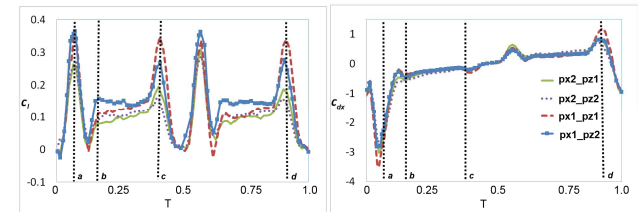

Figure 5. c_l and c_{dx} of one wing of TL_FMAV2 and TL_FMAV4 over one period.

Figure 6. c_{dy} and P_{in} of one wing of TL_FMAV2 and TL_FMAV4 over one period.

Figure 9. c_l and c_{dx} of one wing of WWIM1-px2_pz1, px2_pz2, px1_pz1 and px1_pz2 over one period.
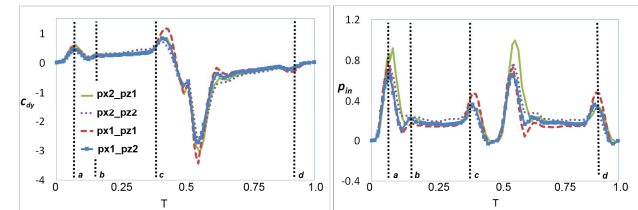

Figure 10. c_{dy} and P_{in} of one wing of WWIM1-px2_pz1, px2_pz2, px1_pz1 and px1_pz2 over one period.

Figure 9 and Figure 10 show the c_l, c_{dx}, c_{dy} and P_{in} of one wing of WWIM1-px2_pz1, px2_pz2, px1_pz1 and px1_pz2 over one period. On average, WWIM1- px1_pz2 gives the highest lift, lowest drag and power input. WWIM1- px1_pz1 also provides high lift but at the expense of high drag. On the other hand, WWIM1- px2_pz1 gives the lowest lift while requiring the highest power. To determine the difference in lift among wings of different flexibility, we look at the various time instants of c_l in Figure 9. At time = 0.08T, corresponding to the dotting line (a), there is a sharp lift increase for all wings, although WWIM1- px1_pz1 and WWIM1- px1_pz2 (spanwise rigid) produce more lift than WWIM1- px2_pz1 and WWIM1- px2_pz2 (spanwise quadratic). The cylindrical sections of the 3D radial vorticity field at radius R = 0.7c are created and then projected on a plane.
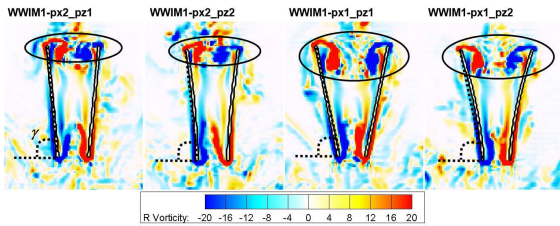

Figure 11. Projected Radial (R) vorticity of WWIM1-px2_pz1, px2_pz2, px1_pz1 and px1_pz2 at radius = 0.7c at time = 0.08T.

Comparing between the different wing flexibility as shown in Figure 11 at time = 0.08T, there is a clear distinction between spanwise rigid (WWIM1- px1_pz1 and WWIM1- px1_pz2) and spanwise flexible (WWIM1- px2_pz1 and WWIM1- px2_pz2) wings. Spanwise rigid wings, which have larger developed LEVs and larger angle of attack (γ, with respect to the horizontal, seeFigure 11), produce higher lift than the flexible ones.
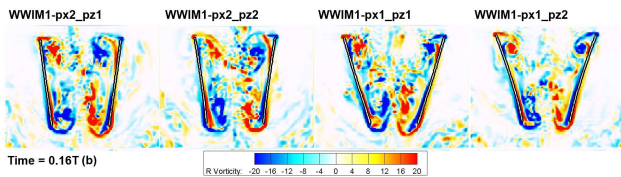

Figure 12. Radial vorticity of WWIM1-px2_pz1, px2_pz2, px1_pz1 and px1_pz2 at radius = 0.7c at time = 0.16T. (b) corresponds to the time instants of the vertical dotted lines in Figure 9 and Figure 10.

We now turn our attention to time = 0.16T (vertical dotted line *b*). It is observed that WWIM1-px1_pz2 produces more lift compared to the rest of the wings. With reference to Figure 12, WWIM1-px1_pz2 has well-defined LEVs attached on the wings' surface, unlike the other three wing deformations. Moreover, its TEVs are also smaller compared to the other three wing deformations. Similar to the previous 2 / 4 wing comparison, the larger LEV and small TEV helps to maintain the vortical asymmetry and increase lift.

The above result shows that the optimum wing configuration would be one which is rigid spanwise and flexible chordwise, since it will provide high lift, low drag and low power requirement. This observation fits the wing design of most current FMAVs, which has an almost rigid carbon rod as the leading edge span, and a highly flexible membrane surface strengthened by thin ribs.

Conclusions

Simulations have been performed using an IBM solver to investigate the underlying aerodynamics of wing-wing interaction (WWI) on a 4-wing flapping wing platform (TL_FMAV4). Results show that TL_FMAV4 produces more than twice the amount of lift compared to TL_FMAV2, but at the expense of

higher drag and power requirement. Depending on mission objective, when there is payload requirement, TL_FMAV4 is still more advantageous since the 2× more lift production can offset the small weight increase and higher payloads. The flexibility study shows that having a rigid spanwise and flexible chordwise wing produces the highest lift, minimum drag and power requirement. This observation fits the wing design of current FMAVs, which has an almost rigid carbon rod as the leading edge span, and a highly flexible membrane surface strengthened by thin ribs.

References

[1]   T. Weis-Fogh, Quick estimates of flight fitness in hovering animals, including novel mechanisms for lift production. *The Journal of Experimental Biology*. vol. 59. 1973. pp. 169–230.

[2]   K.M.E. De Clercq, R. De Kat, B. Remes, B.W. van Oudheusden, and H. Bijl, Aerodynamic experiments on Delfly II : Unsteady lift enhancement. *International Journal of Micro Air Vehicles*. vol. 1. 2009. pp. 255–262.

[3]   Q. V Nguyen, W.L. Chan, and M. Debiasi, Development of an Insect-Inspired Flapping-Wing Micro Air Vehicle Capable of Vertical Take-off and Hovering, *International Conference on Intelligent Robots and Systems*, Chicago, Illinois: 2014.

[4]   L. a Miller and C.S. Peskin, Flexible clap and fling in tiny insect flight. *The Journal of experimental biology*. vol. 212. Oct. 2009. pp. 3076–90.

[5]   R. Mittal and G. Iaccarino, Immersed boundary methods. *Annual Review of Fluid Mechanics*. vol. 37. Jan. 2005. pp. 239–261.

[6]   W.B. Tay, B.W. van Oudheusden, and H. Bijl, Numerical simulation of X-wing type biplane flapping wings in 3D using the immersed boundary method. *Bioinspiration & biomimetics*. vol. 9. Mar. 2014. p. 036001.

[7]   L. a Miller and C.S. Peskin, When vortices stick: an aerodynamic transition in tiny insect flight. *The Journal of experimental biology*. vol. 207. Aug. 2004. pp. 3073–88.

[8]   D. Kolomenskiy, H.K. Moffatt, M. Farge, and K. Schneider, Two- and three-dimensional numerical simulations of the clap–fling–sweep of hovering insects. *Journal of Fluids and Structures*. vol. 27. Jul. 2011. pp. 784–791.